Allometric growth in the frontals of the Mongolian theropod dinosaur *Tarbosaurus bataar*

CHAN-GYU YUN, GALADRIEL FREEMAN PETERS, and PHILIP JOHN CURRIE

Yun, C.-G., Peters, G.F., and Currie, P.J. 2022. Allometric growth in the frontals of the Mongolian theropod dinosaur *Tarbosaurus bataar*. *Acta Palaeontologica Polonica* 67 (3): 601–615.

Tarbosaurus bataar is a sister taxon of the well-studied theropod dinosaur *Tyrannosaurus rex*, and numerous fossils of this tyrannosaurid have been discovered in the Upper Cretaceous Nemegt Formation of Mongolia. Although specimens of different sizes of *Tarbosaurus bataar* have been discovered since its initial description, few rigorous studies on its growth changes have been done. Here we examine growth changes in the frontal bones of seven *Tarbosaurus bataar* specimens using bivariate analyses and the Björk superimposition method to demonstrate trends in their ontogenetic allometry. The width and depth of the frontal undergoes positive allometry during growth, whereas the length shows a trend of negative allometry. The details of growth changes in *Tarbosaurus bataar* frontals are largely similar to those of *Tyrannosaurus rex*. Furthermore, generic allometric trends of tyrannosaurid frontals, including those of *Tarbosaurus bataar*, are shared with other large-bodied theropod clades and may represent a consequence of strengthening parts of the braincase as an anchor for the jaw musculature.

Key words: Dinosauria, Theropoda, Tyrannosauridae, *Tarbosaurus bataar*, *Tyrannosaurus rex*, frontal, ontogeny, allometry.

Chan-Gyu Yun [changyu1015@naver.com], Biological Sciences, Inha University, Incheon 22212, Republic of Korea. Galadriel Freeman Peters [freemanp@ualberta.ca] and Philip John Currie [philip.currie@ualberta.ca], Department of Biological Sciences, University of Alberta, Edmonton, Alberta, T6G 2E9, Canada.

Received 27 September 2021, accepted 24 March 2022, available online 17 August 2022.

Introduction

From 1946 to 1949, many fossils of a theropod clade now known as Tyrannosauridae were collected from the Nemegt Formation (?Maastrichtian) of the Gobi Desert by the Mongolian Paleontological Expedition of the USSR Academy of Sciences (Maleev 1955b). Maleev (1955a) described and designated one specimen (PIN 551-1) from these expeditions as the holotype of a new taxon (*Tyrannosaurus bataar*), and in a nearly simultaneous publication three specimens (PIN 551-2, 552-2, 553-1) became the holotypes of *Tarbosaurus efremovi*, *Gorgosaurus lancinator*, and *Gorgosaurus novojilovi* (Maleev 1955b). Later, Rozhdestvensky (1965) recognized that these four tyrannosaurid taxa represented a single species, of which *Tyrannosaurus bataar* would have priority. However, he considered the Mongolian tyrannosaur different enough to be classified as a distinct genus from *Tyrannosaurus* and introduced the combination *Tarbosaurus bataar*. Although there are some researchers who still consider *Tarbosaurus* a junior synonym of *Tyrannosaurus* by following the taxonomic practice of treating sister species as congeneric (Carr et al. 2017; Delcourt and Grillo 2018; Carr 2020), many workers on Tyrannosauridae do not accept this synonymy as there are enough morphological differences to distinguish *Tarbosaurus* from *Tyrannosaurus* (Currie 2003b; Hurum and Sabath 2003). *Tarbosaurus bataar* has fallen into many different positions in recent phylogenetic analyses: as a sister taxon of the smaller contemporaneous tyrannosaurid *Alioramus remotus* (Currie et al. 2003), although this is disputed (Brusatte et al. 2012; Lü et al. 2014); as a sister taxon of another large Asian tyrannosaurid *Zhuchengtyrannus magnus* (Loewen et al. 2013; Fiorillo and Tykoski 2014), although recent studies have disputed these results (e.g., Brusatte and Carr 2016); and as a sister taxon of the North American *Tyrannosaurus rex* (Brusatte and Carr 2016; Carr et al. 2017). Recently, Paul et al. (2022) suggested that several specimens originally assigned to *Tyrannosaurus rex* belong to two distinct species and named them as *Tyrannosaurus imperator* and *Tyrannosaurus regina*. While we do not consider these species as valid (reassessment of the two proposed species is beyond the scope of this work), it nevertheless opens the possibility that the sister species relationship between *Tarbosaurus bataar* and *Tyrannosaurus*

rex could be questionable depending on potential new discoveries. Furthermore, a recent study found the ages of large tyrannosaurine specimens from the southern regions of North America, previously referred to the late Maastrichtian *Tyrannosaurus rex*, in fact significantly predate this taxon as they are constrained to the latest Campanian or earliest Maastrichtian. This potentially supports the distinctiveness of such specimens (Dalman et al. 2022). As generic distinction of *Tarbosaurus* and *Tyrannosaurus* gives more room for the assessment of relationships of such specimens, it may be more appropriate to treat these genera as separate. After the description and naming of the taxon by Maleev (1955a), many additional specimens of *Tarbosaurus bataar* have been discovered (Hurum and Sabath 2003; Currie 2009, 2013, 2016; Jerzykiewicz et al. 2021) and these have been the subjects of many anatomical studies (Hurum and Sabath 2003; Saveliev and Alifanov 2007; Tsuihiji et al. 2011). However, despite this wealth of material, little is known about the ontogeny of this Mongolian tyrannosaurid. This contrasts with its North American relatives in which growth series are known (Carr 1999, 2010; Currie 2003a; Carr and Williamson 2004; Voris et al. 2019) and growth trends have been thoroughly described (Russell 1970; Currie 1987; Carr 1999, 2020). The description of *Tarbosaurus bataar* ontogeny provided by Rozhdestvensky (1965) is brief and mainly focused on proportions and "robustness" of some skeletal parts. A well-preserved, small, two- to three-year-old individual (MPC-D 107/07) was reported by Tsuihiji et al. (2011), and there are other possible cases of similarly aged young *Tarbosaurus bataar* (Currie and Dong 2001; Sereno et al. 2009; Fowler et al. 2011). However, these cases represent a very early part of ontogeny, and specimens of larger sizes (large juveniles, subadults) have not been described to fill in the gap between young and mature growth stages.

Frontals are paired bones that form the anterodorsal part of the braincase. The frontal is considered one of the most taxonomically informative bones among theropods (Currie 1987; Longrich 2008; Averianov 2016). Additionally, due to their compact nature, theropod frontals are better represented in the fossil record than other cranial bones, making them some of the most important skeletal parts for understanding theropod paleobiology (Currie 1987; Averianov 2016). Frontals of tyrannosaurids have been described in detail (Lehman and Wick 2012; McDonald et al. 2018; Yun 2020b, 2022; Paulina-Carabajal et al. 2021), and a considerable amount of ontogenetic variation of this element has been recognized (Currie 2003b; Lehman and Wick 2012; Carr 2020; Yun 2020b). However, most of these studies focused on North American taxa, and it is still debated whether the peculiar morphologies of some specimens represent ontogenetic or intraspecific variation, or phylogenetic signals (McDonald et al. 2018; Voris et al. 2020; Yun 2020a, b). Furthermore, most of these studies focus on character changes, and allometric scaling in various parts of the frontal has received less attention. Currie (2003a, b) described allometric growth trends of various skeletal parts of tyrannosaurids, but only limited dimensions (depth, length and width of the bone) were compared from frontals. Thus, any new data about ontogenetic allometry or trends in tyrannosaurid frontals, especially those of Asian taxa, are particularly important.

Here, the ontogenetic allometry of the frontal in *Tarbosaurus bataar* is described, based on seven specimens of different sizes from the Nemegt Formation that are housed in the Institute of Paleontology of the Mongolian Academy of Sciences in Ulaanbaatar, Mongolia. These specimens, as well as MPC-D 107/07, were included in multiple allometric analyses to determine which parts of the frontal grew slower or faster as the animals increased in size. Furthermore, some of these analyses are supplemented with superimposition of bone silhouettes through the Björk method of superimposition.

Institutional abbreviations.—CMNH, Cleveland Museum of Natural History, Cleveland, USA; FSAC, Faculté des Sciences Aïn Chock, Casablanca, Morocco; LACM, Natural History Museum of Los Angeles County, Los Angeles, USA; MCF, Museo Carmen Funes, Plaza Huincul, Argentina; MPC, Institute of Paleontology and Geology of the Mongolian Academy of Sciences, Ulaanbaatar, Mongolia; PIN, Palaeontological Institute of the Russian Academy of Sciences, Moscow, Russia.

Other abbreviations.—P, p-value; R^2, R squared coefficient of determination.

Material and methods

Measurements and silhouettes for the Björk superimposition method (e.g., Carpenter 2010) were made of MPC-D 107/05, 06, 09–11, 13, 22 from images photographed from the original specimens for this purpose by PJC (Fig. 1), and from the published figures of MPC-D 107/07 by Tsuihiji et al. (2011). A total of eight specimens were included in the analysis, although some measurements were unavailable for some specimens. Although the sample size is admittedly small, which may introduce some limitations (Brown and Vavrek 2015), the current dataset comprises a wide range of sizes that make it sufficient, especially given that this is based on fossils (Hone et al. 2016b). Use of images to test the allometric relationship between variables is a valid method (e.g., Hone et al. 2016) that yields very similar results to those of an allometric study using three-dimensional geometric morphometric analysis (e.g., Knapp et al. 2021).

The measurements used in this study (Table 1) are as follows: (1) width of the base of the nasal process; (2) width of the prefrontal suture on the dorsal or ventral surface; (3) width of the lacrimal socket; (4) length of the frontal between prefrontonasal process and the frontoparietal suture; (5) width of the frontal between medial edge of the orbital slot and the midline; (6) width of the frontal between the most lateral point of the posterior shelf and the midline;

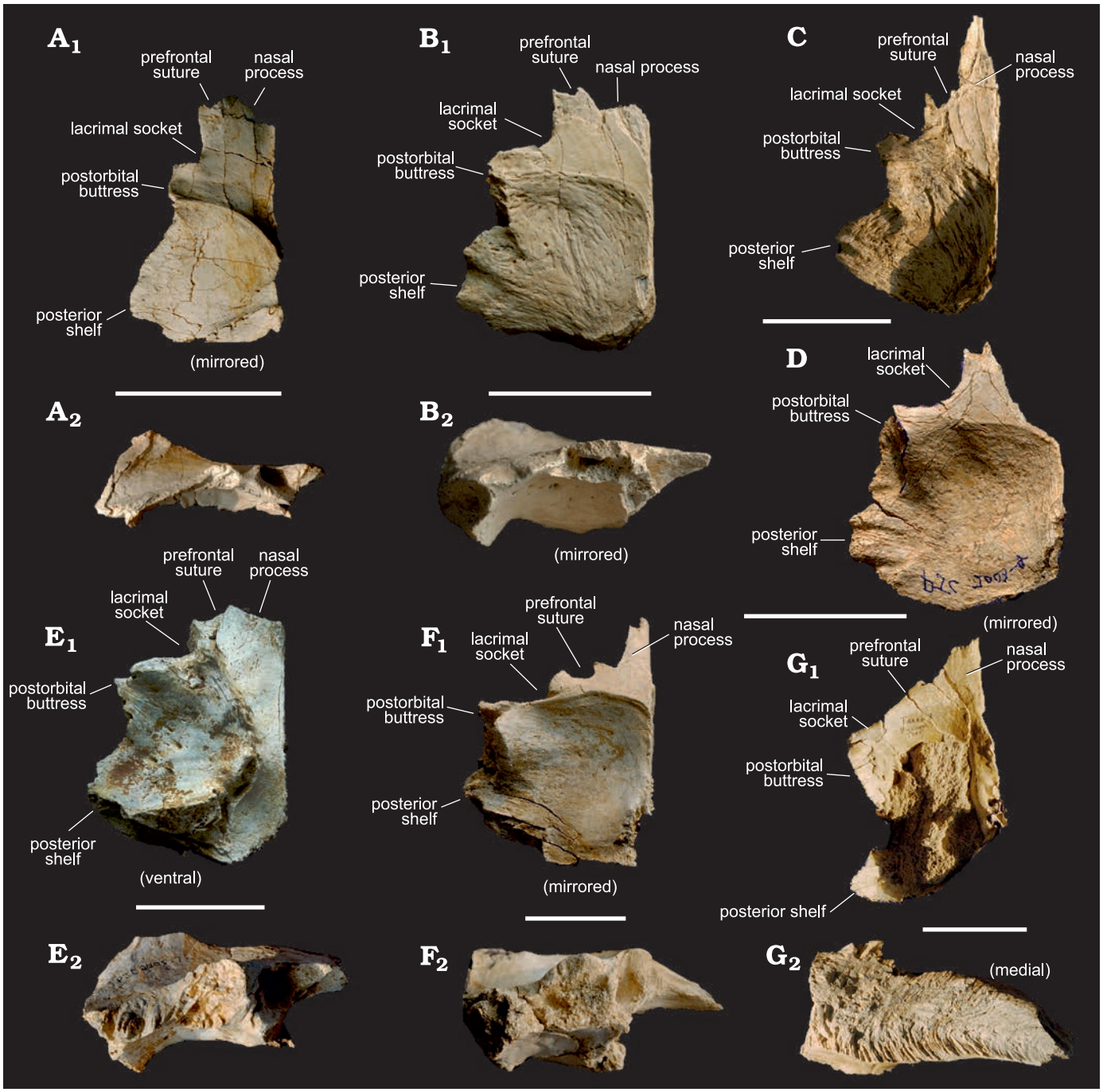

Fig. 1. Tyrannosaurid theropod *Tarbosaurus bataar* Maleev, 1955a from Mongolia, Nemegt Formation, Maastrichtian; frontals used to create bone silhouettes for superimposition. **A**. MPC-D 107/10, from Bugiin Tsav, in dorsal (A_1) and lateral (A_2) views. **B**. MPC-D 107/09, Bugiin Tsav, in dorsal (B_1) and lateral (B_2) views. **C**. MPC-D 107/05, Nemegt, in dorsal view. **D**. MPC-D 107/11, Bugiin Tsav, in dorsal view. **E**. MPC-D 107/13, Nemegt, in dorsal (E_1) and lateral (E_2) views. **F**. MPC-D 107/22, Bugiin Tsav, in dorsal (F_1) and lateral (F_2) views. **G**. MPC-D 107/06, Bugiin Tsav, in dorsal (G_1) and medial (G_2) views. The arrangement is from smallest to largest. Scale bars 50 mm.

(7) length of the dorsotemporal fossa between the middle of the dorsotemporal ridge and the frontoparietal suture; (8) length of the brain between most anterior point of the olfactory bulb fossa and the most posterior point of the cerebral fossa; (9) depth of the frontal at the region that is immediately anterior to the most anterior point of the sagittal crest; (10) length of the postorbital suture between the most anterior point of the anterior part and the most posterior point of the posterior part of the suture; (11) dorsoventral depth of the anterior part of the postorbital suture; (12) dorsoventral depth of the posterior part of the postorbital suture (Fig. 2). Note that the postorbital suture of the frontal has two distinct regions, which is why two measurements (Fig. 2: 11, 12) were taken. The anterior part of the postorbital suture is usually taller, narrower, and oriented more laterally than the posterior part of the postorbital suture.

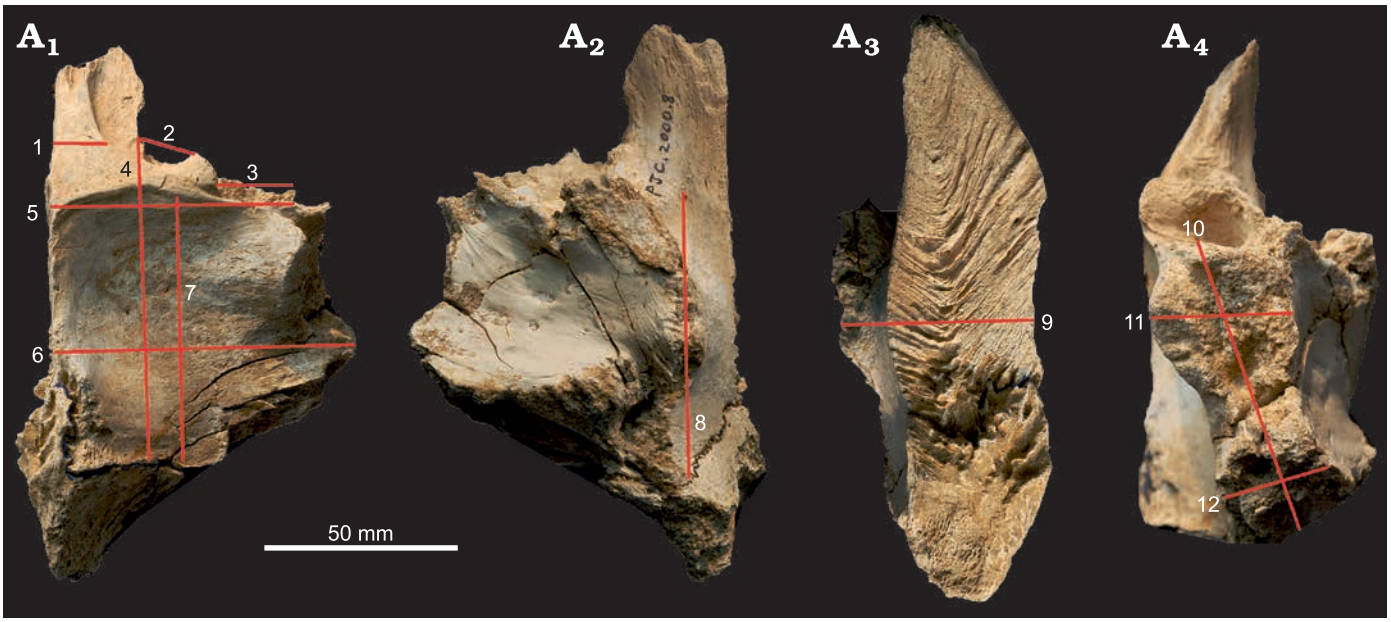

Fig. 2. Measurement parameters used in study, with frontal of *Tarbosaurus bataar* Maleev, 1955a (MPC-D 107/22), from Bugiin Tsav, Nemegt Formation, Maastrichtian, as an example. Measurement parameters in dorsal (A_1), ventral (A_2), medial (A_3), and lateral (A_4) views. 1, width of the nasal process; 2, width of the prefrontal suture; 3, width of the lacrimal socket; 4, length of the frontal between prefrontonasal process and the frontoparietal suture; 5, width of the frontal between medial edge of the orbital slot and the midline; 6, width of the frontal between the most lateral point of the posterior shelf and the midline; 7, length of the dorsotemporal fossa between the middle of the dorsotemporal ridge and the frontoparietal suture; 8, length of the brain between most anterior point of the olfactory bulb fossa and the most posterior point of the cerebral fossa; 9, depth of the frontal at the region that is immediately anterior to the most anterior point of the sagittal crest; 10, length of the postorbital suture between the most anterior point of the anterior part and the most posterior point of the posterior part of the suture; 11, dorsoventral depth of the anterior part of the postorbital suture; 12, dorsoventral depth of the posterior part of the postorbital suture. The same numbers appear in Figs. 3–5 and Table 1.

Table 1. Measurements (in mm) of *Tarbosaurus bataar* frontals used in the analyses. Log transformed measurements are in parentheses. 1, width of the nasal process; 2, width of the prefrontal suture; 3, width of the lacrimal socket; 4, prefrontolacrimal process-frontoparietal suture length; 5, width of the frontal between medial edge of the orbital slot and the midline = orbital slot to the midline width; 6, width of the frontal between the most lateral point of the posterior shelf and the midline = lateralmost part of the posterior shelf to the midline width; 7, length of the dorsotemporal fossa between the middle of the dorsotemporal ridge and the frontoparietal suture = dorsotemporal fossa length; 8, length of the brain between most anterior point of the olfactory bulb fossa and the most posterior point of the cerebral fossa = brain length; 9, depth of the bone; 10, length of the postorbital suture between the most anterior point of the anterior part and the most posterior point of the posterior part of the suture = postorbital suture length; 11, dorsoventral depth of the anterior part of the postorbital suture = anterior part of the postorbital suture depth; 12, dorsoventral depth of the posterior part of the postorbital suture = posterior part of the postorbital suture depth; L, left; N/A, not available; R, right.

Specimen	Position	1	2	3	4	5	6	7	8	9	10	11	12	Source
MPC-D 107/05	L	19.4 (1.29)	9.3 (0.97)	9.8 (0.99)	88.0 (1.94)	46.1 (1.66)	63.4 (1.8)	60.6 (1.78)	N/A	N/A	41.6 (1.62)	N/A	N/A	PJC (unpublished data)
MPC-D 107/06	L	28.4 (1.45)	29.6 (1.47)	32.8 (1.52)	125.6 (2.1)	89.9 (1.95)	97.4 (1.99)	117.1 (2.07)	89.7 (1.95)	71.9 (1.86)	84.8 (1.93)	N/A	N/A	PJC (unpublished data)
MPC-D 107/07	L	10.6 (1.03)	6.0 (0.78)	4.0 (0.6)	58.6 (1.77)	19.0 (1.28)	20.3 (1.31)	28.5 (1.45)	N/A	N/A	27.9 (1.45)	5.1 (0.71)	4.0 (0.6)	Tsuihiji et al. 2011
MPC-D 107/09	L	14.8 (1.17)	7.7 (0.89)	15.5 (1.19)	79.7 (1.9)	50.6 (1.7)	64.2 (1.81)	49.1 (1.69)	63.2 (1.8)	27.8 (1.44)	45.4 (1.66)	12.6 (1.1)	8.3 (0.92)	PJC (unpublished data)
MPC-D 107/10	R	16.4 (1.21)	6.0 (0.78)	6.2 (0.79)	76.4 (1.88)	30.3 (1.48)	45.5 (1.66)	40.5 (1.61)	65.1 (1.81)	14.19 (1.15)	43.8 (1.64)	8.4 (0.92)	4.4 (0.64)	PJC (unpublished data)
MPC-D 107/11	R	N/A	N/A	19.9 (1.3)	93.8 (1.97)	59.1 (1.77)	76.2 (1.88)	64.1 (1.81)	66.4 (1.82)	N/A	54.6 (1.74)	N/A	N/A	PJC (unpublished data)
MPC-D 107/13	R	20.9 (1.32)	14.3 (1.16)	24.5 (1.39)	96.0 (1.98)	60.2 (1.78)	76.7 (1.88)	64.6 (1.81)	84.5 (1.93)	35.1 (1.55)	52.5 (1.72)	24.2 (1.38)	15.6 (1.19)	PJC (unpublished data)
MPC-D 107/22	R	21.4 (1.33)	21.3 (1.33)	24.0 (1.38)	106.6 (2.03)	80.0 (1.9)	92.5 (1.97)	93.4 (1.97)	94.1 (1.97)	60.2 (1.78)	66.2 (1.82)	31.8 (1.5)	26.6 (1.42)	PJC (unpublished data)

Details regarding some landmarks used for these measurements are presented in Currie (2003b) and Evans et al. (2017). For the specimens that lack a prefrontonasal process, the anteromedial part of the joint surface for the prefrontal was used as a landmark; for the specimens in which the lateral views were not available, measurements were taken from the dorsal or ventral views. Measurements were taken using the program ImageJ (Schneider et al. 2012), and these were rounded to two decimal places. To linearize relationships, these measurements were log-transformed and rounded to three decimal places and evaluated for allometry using a principle of Standardized Major Axis (SMA) regression as it assumes that both variables contain errors (Warton et al. 2006). Regression analyses (Figs. 3–5; Table 2) were done and associated statistics—such as slopes, intercepts, 95% confidence intervals, or coefficients of determination (R^2)—were obtained by the linear regression calculator of GraphPad (https://www.graphpad.com). Positive allometry is demonstrated when the slope is significantly more than 1.0, or when the 95% confidence interval of slope is more

Table 2. Allometric regressions of *Tarbosaurus bataar* frontal ontogeny. Regression formulas expressed as log (y) = m · log (x) + b. N, number of specimens.

Comparison (x : y)	N	Slope (m)	95% CI (m)	Intercept (b)	95% CI (b)	R^2	Allometry
Width between the orbital slot and the midline: Length between the prefrontonasal process and the frontoparietal suture	8	0.4372	0.3148–0.5597	1.207	0.9988–1.416	0.9271	negative
Width between the lateralmost part of the posterior shelf and the midline: Length between the prefrontonasal process and the frontoparietal suture	8	0.4258	0.2624–0.5892	1.185	0.8911–1.479	0.8714	negative
Width between the lateralmost part of the posterior shelf and the midline: Width between the orbital slot and the midline	8	0.9784	0.7513–1.206	-0.059	-0.4677–0.3498	0.9488	isometry
Length between the prefrontonasal process and the frontoparietal suture: Width of the nasal process	7	1.224	0.9119–1.536	-1.12	-1.727–-0.5138	0.9532	isometry
Width between the orbital slot and the midline: Width of the nasal process	7	0.5188	0.2396–0.7979	0.3864	-0.08615–0.8539	0.8203	negative
Length between the prefrontonasal process and the frontoparietal suture: Width of the prefrontal suture	7	2.383	1.397–3.368	-3.575	-5.492–1.658	0.8854	positive
Width between the orbital slot and the midline: Width of the prefrontal suture	7	1.043	0.4679–1.619	-0,6969	-1.671–0.2770	0.8130	isometry
Length between the prefrontonasal process and the frontoparietal suture: Width of the lacrimal socket	8	2.968	1.703–4.234	-4.632	-7.098–-2.166	0.8459	positive
Width between the orbital slot and the midline: Width of the lacrimal socket	8	1.427	1.094–1.760	-1.267	-1.833–-0.7005	0.9484	positive
Length between the prefrontonasal process and the frontoparietal suture: Length of the brain	6	0.807	0.09824–1.516	0.2848	-1.117–1.687	0.7141	isometry
Length between the prefrontonasal process and the frontoparietal suture: Width between the orbital slot and the midline	8	2.120	1.526–2.714	-2.437	-3.594–-1.280	0.9271	positive
Length between the prefrontonasal process and the frontoparietal suture: Width between the lateralmost part of the posterior shelf and the midline	8	2.046	1.261–2.832	-2.195	-3.726–-0.6652	0.8714	positive
Length between the prefrontonasal process and the frontoparietal suture: Length of the dorsotemporal fossa	8	1.941	1.701–2.181	-2.003	-2.471–-1.535	0.9849	positive
Width between the orbital slot and the midline: Length of the dorsotemporal fossa	8	0.8559	0.6199–1.092	0.3272	-0.07455–0.7290	0.9292	isometry
Length between the prefrontonasal process and the frontoparietal suture: Length of the postorbital suture	8	1.392	1.060–1.724	-1.012	-1.659–-0.3648	0.9461	positive
Width between the orbital slot and the midline: Depth of the bone anterior to the sagittal crest	5	1.518	1.265–1.772	-1.119	-1.568–-0.6701	0.9918	positive
Length between the prefrontonasal process and the frontoparietal suture: Depth of the bone anterior to the sagittal crest	5	2.931	1.050–4.813	-4.242	-7.968–-0.5168	0.8912	positive
Length between the prefrontonasal process and the frontoparietal suture: Depth of the anterior part of the postorbital suture	5	3.194	2.121–4.268	-4.985	-7.040–-2.930	0.9676	positive
Length between the prefrontonasal process and the frontoparietal suture: Depth of the posterior part of the postorbital suture	5	3.304	1.002–5.606	-5.363	-9.769–-0.9575	0.8743	positive
Depth of the anterior part of the postorbital suture: Depth of the posterior part of the postorbital suture	5	1.063	0.6373–1.489	-0.2389	-0.7325–0.2547	0.9546	isometry
Depth of the bone anterior to the sagittal crest: Depth of the anterior part of the postorbital suture	4	0.9688	0.1330–1.805	-0.2089	-1.460–1.043	0.9256	isometry
Depth of the bone anterior to the sagittal crest: Depth of the posterior part of the postorbital suture	4	1.272	0.6402–1.904	-0.8403	-1.787–0.1060	0.9740	isometry

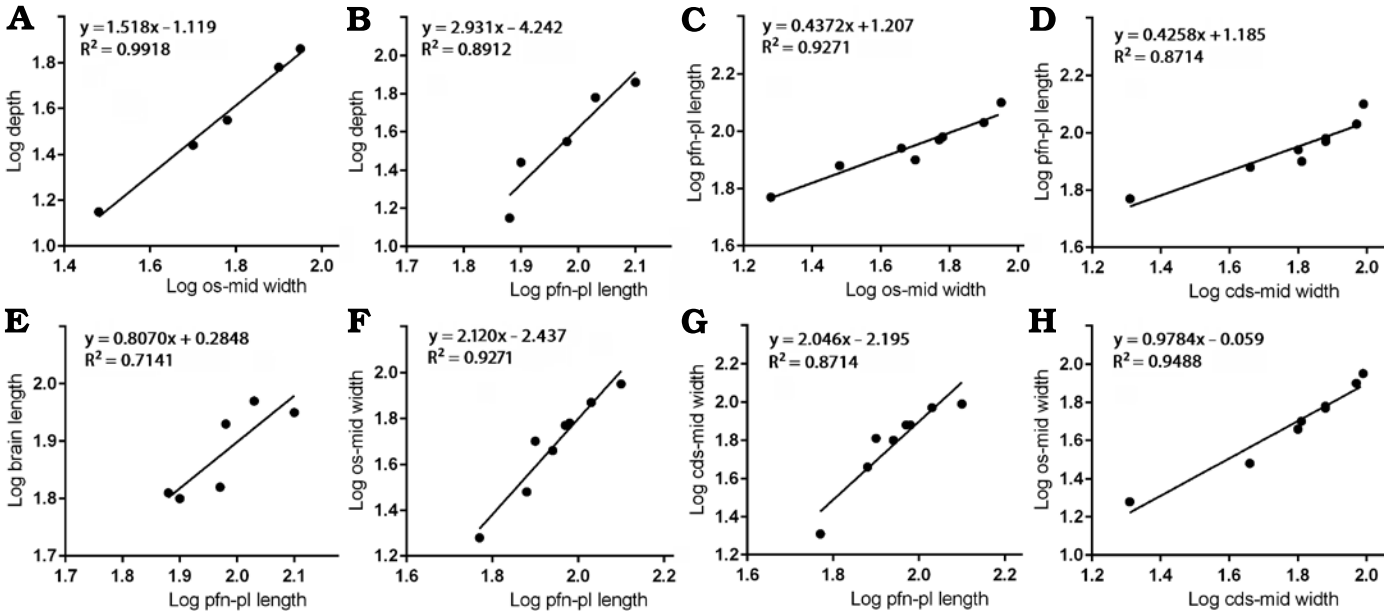

Fig. 3. Bivariate allometric results of different parts of *Tarbosaurus bataar* frontals. **A**. Width of the frontal between medial edge of the orbital slot and the midline (os-mid width, 5) and the depth of the frontal at the region that is immediately anterior to the most anterior point of the sagittal crest (depth, 9). **B**. Length of the frontal between prefrontonasal process and the frontoparietal suture (pfn-pl length, 4) and the depth of the frontal at the region that is immediately anterior to the most anterior point of the sagittal crest (9). **C**. Width of the frontal between medial edge of the orbital slot and the midline (5) and the length of the frontal between prefrontonasal process and the frontoparietal suture (4). **D**. Length of the frontal between prefrontonasal process and the frontoparietal suture (4) and the width of the frontal between the most lateral point of the posterior shelf and the midline (cds-mid width, 6). **E**. Length of the frontal between prefrontonasal process and the frontoparietal suture (4) and the brain length (8). **F**. Length of the frontal between prefrontonasal process and the frontoparietal suture (4) and the width of the frontal between medial edge of the orbital slot and the midline (5). **G**. Length of the frontal between prefrontonasal process and the frontoparietal suture (4) and the width of the frontal between the most lateral point of the posterior shelf and the midline (6). **H**. Width of the frontal between the most lateral point of the posterior shelf and the midline (6) and the width of the frontal between medial edge of the orbital slot and the midline (5).

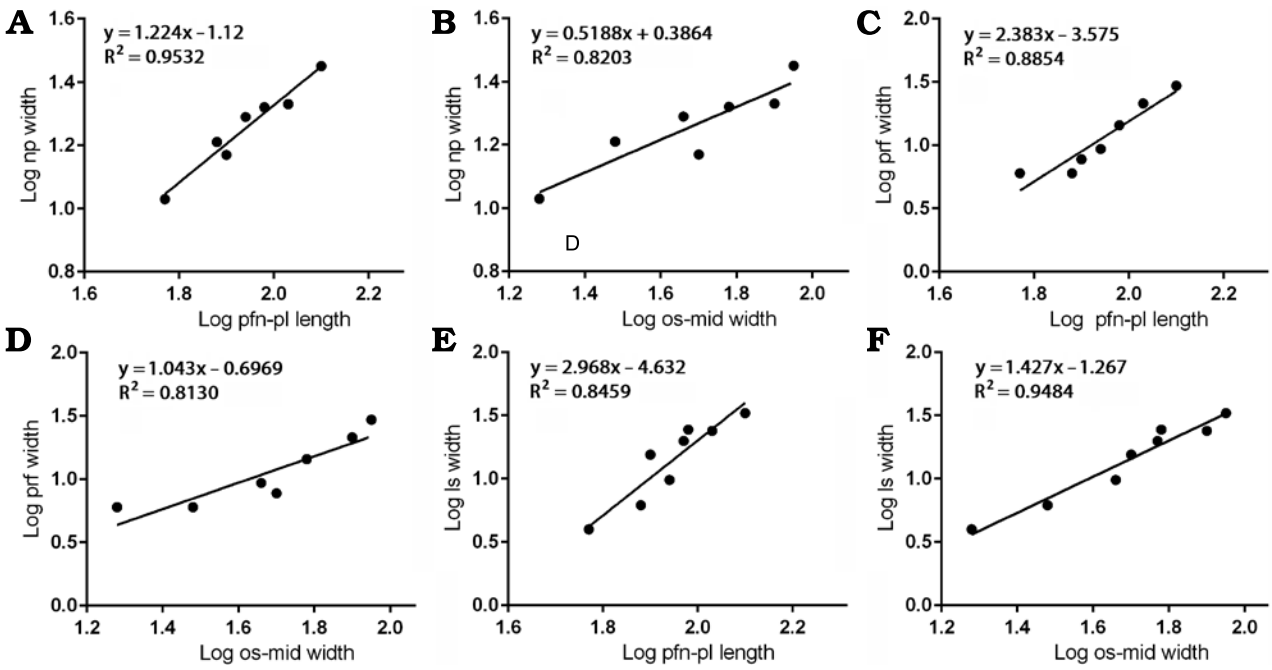

Fig. 4. Bivariate allometric results of different parts of *Tarbosaurus bataar* frontals. **A**. Length of the frontal between prefrontonasal process and the frontoparietal suture (pfn-pl length, 4) and the width of the nasal process (np width, 1). **B**. Width of the frontal between medial edge of the orbital slot and the midline (os-mid width, 5) and the width of the nasal process (1). **C**. Length of the frontal between prefrontonasal process and the frontoparietal suture (4) and the width of the prefrontal suture (prf width, 2). **D**. Width of the frontal between medial edge of the orbital slot and the midline (5) and the width of the prefrontal suture (2). **E**. Length of the frontal between prefrontonasal process and the frontoparietal suture (4) and the width of the lacrimal socket (ls width, 3). **F**. Width of the frontal between medial edge of the orbital slot (5) and the midline and the width of the lacrimal socket (3).

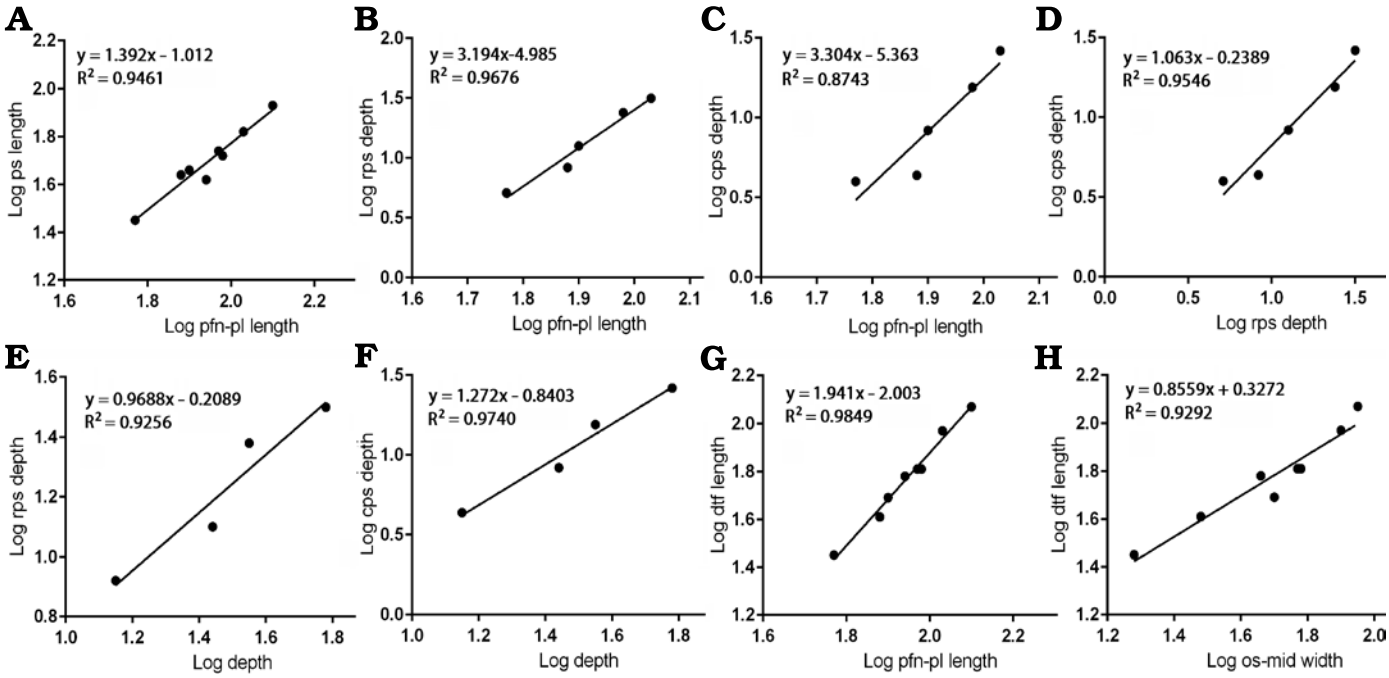

Fig. 5. Bivariate allometric results of different parts of *Tarbosaurus bataar* frontals. **A**. Length of the frontal between prefrontonasal process and the frontoparietal suture (pfn-pl length, 4) and the length of the postorbital suture (ps length, 10). **B**. Length of the frontal between prefrontonasal process and the frontoparietal suture (4) and the depth of the anterior part of the postorbital suture (rps depth, 11). **C**. Length of the frontal between prefrontonasal process and the frontoparietal suture (4) and the depth of the posterior part of the postorbital suture (cps depth, 12). **D**. Depth of the anterior part of the postorbital suture (11) and the depth of the posterior part of the postorbital suture (12). **E**. Depth of the frontal at the region that is immediately anterior to the most anterior point of the sagittal crest (depth, 9) and the depth of the anterior part of the postorbital suture (11). **F**. Depth of the frontal at the region that is immediately anterior to the most anterior point of the sagittal crest (9) and the depth of the posterior part of the postorbital suture (12). **G**. Length of the frontal between prefrontonasal process and the frontoparietal suture (4) and the length of the dorsotemporal fossa (dtf length, 7). **H**. Width of the frontal between medial edge of the orbital slot and the midline (os-mid width, 5) and the length of the dorsotemporal fossa (7).

than 1.0. When the slope is significantly less than 1.0 (or the 95% confidence interval of slope is less than 1.0), it is considered as negative allometry. When the slope is 1.0 or very close to it, or when 1.0 falls within the range of the 95% confidence interval of slope, growth is considered as isometric. Some of these analyses are supplemented by the Björk superimposition method on the dorsal and ventral or lateral and medial views (Figs. 6, 7), as this method allows visualization of regions of ontogenetic changes or allometric growth, and permits utilization of incomplete specimens without having to estimate (fabricate) missing data (Carpenter 2010). This method of superimposing silhouettes of bone has been demonstrated to be useful in ontogenetic variation studies of dinosaurs (Carpenter 2010). Furthermore, the Björk method of superimposition is useful in critically examining the results of bivariate analyses (Carpenter 2010). MPC-D 107/07 was not included in the Björk method of superimposition, and MPC-D 107/05 and MPC-D 107/11 were excluded in superimposing lateral/medial silhouettes due to lack of images.

The anatomical nomenclature used in this study follows Currie (2003b), Carr et al. (2017), McDonald et al. (2018) and Yun (2020b), except that the term "posterior shelf" is used instead of "caudal shelf" (sensu Carr et al. 2017) for an area that is directly anterior to the parietal suture, which is defined laterally by the posterior part of the postorbital suture.

Taxonomic referral.—Because the Nemegt Formation has two contemporary tyrannosaurids, *Alioramus remotus* and *Tarbosaurus bataar* (Currie 2003b; Brusatte et al. 2012; Carr et al. 2017), referral of the specimens discussed in this work to *Tarbosaurus bataar* needs to be justified. The majority of the specimens (MPC-D 107/05, 06, 09, 11, 13, 22) share several characters that suggest derived tyrannosaurine affinity. These include a long and tall sagittal crest, and a rectangular main body of the frontal formed by a wide postorbital buttress and posterior shelf (Currie 2003b; Carr and Williamson 2004). These are present in larger specimens of *Tarbosaurus bataar* (Hurum and Sabath 2003) but are very different in *Alioramus remotus*, which has a triangular frontal with a relatively low, short sagittal crest (Bever et al. 2013). Establishing a taxonomic identity of MPC-D 107/10, the smallest specimen in the sample, is difficult as overall morphology and proportions of this specimen are similar to both *Alioramus remotus* (Bever et al. 2013) and a juvenile *Tarbosaurus bataar* (Tsuihiji et al. 2011). Given the exceptional rarity of *Alioramus remotus* fossils in the Nemegt Formation (Currie 2009, 2013, 2016), which is dissimilar to the abundance of *Tarbosaurus bataar* material, this specimen is provisionally referred to the latter taxon. Based on these reasons, all the specimens described in this work are referred to as a single taxon, *Tarbosaurus bataar*.

Results

Frontal depth.—The depth of the frontal in the region that is immediately anterior to the sagittal crest compared to the width between the orbital slot and the midline shows positive allometry (Fig. 3A) with a slope of 1.518 and a high correlation coefficient (R^2 = 0.9918, P = 0.0003). When the same measurement is compared to the length between the prefrontonasal process and the frontoparietal suture (Fig. 3B), a positive slope (2.931) with a high correlation coefficient (R^2 = 0.8912, P = 0.0158) results. These suggest the depth of the bone significantly increased during growth.

The visual comparisons through the Björk superimposition method support the results of bivariate analyses. Superimpositions of silhouettes in lateral/medial views scaled to the same lengths between the prefrontal suture to the frontoparietal suture show a remarkable increase of the relative depth during growth (Fig. 7A, B).

Frontal length and brain length.—Regression of the length between the prefrontonasal process and the frontoparietal suture against the width between the orbital slot and the midline (Fig. 3C) resulted in a negative slope (0.4372) with significant correlation (R^2 = 0.9271, P = 0.0001). Regression of the length between the prefrontonasal process and the frontoparietal suture against the width between the most lateral part of the posterior shelf and the midline (Fig. 3D) also resulted in a negative slope (0.4258) and the coefficient of determination (R^2) was high (0.8714) and significant (P = 0.0007). As the animal's size increases, therefore, the length of the frontal shortens relative to the rest of the bone. While the slope of the regression of brain length against the length of the bone between the prefrontonasal process and the frontoparietal suture (Fig. 3E) was less than 1 (0.8070), the range of 95% confidence intervals includes 1 (0.09824 to 1.516) with a high correlation coefficient (R^2 = 0.7141, P = 0.0342). This indicates the length of the brain scaled isometrically with the length of the frontal.

Results of Björk method of superimposition are consistent with those of bivariate analyses. When silhouettes from dorsal/ventral and lateral/medial views scaled to the same width and depth are superimposed, a decrease in relative length is observed (Figs. 6, 7).

Frontal width.—The width between the orbital slot and the midline and the width of the posterior shelf against the length between the prefrontonasal process and the frontoparietal suture showed strong positive allometry. The former (Fig. 3F) resulted in a slope of 2.120 (R^2 = 0.9271, P = 0.0001) and the latter (Fig. 3G) with a slope of 2.046 (R^2 = 0.8714, P = 0.0007). These results suggest that as frontal length increases, the width of the frontal becomes larger relative to the rest of the bone. We demonstrate here that the width of the posterior shelf increased isometrically (Fig. 3H) compared with the width between the orbital slot and the midline (slope = 0.9784 with the range of 95% confidence intervals 0.7513 to 1.206), and a correlation coefficient for this was high as well (R^2 = 0.9488, P < 0.0001).

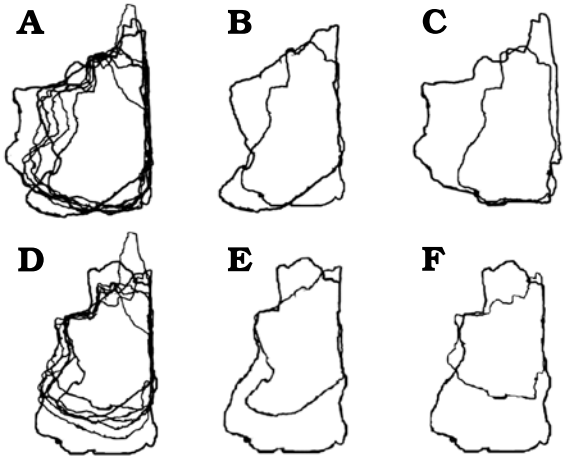

Fig. 6. Björk method of superimposition of the frontals in dorsal/ventral views. **A**. Scaled to same length between prefrontonasal process and the frontoparietal suture. **B**. Smallest and largest specimen superimposed. **C**. Smallest and second largest specimen superimposed. **D**. Scaled to same width between medial edge of the orbital slot and the midline. **E**. Smallest and largest specimen superimposed. **F**. Smallest and second largest specimen superimposed. Largest specimens preserve entire nasal process, which emphasize relative shortening during growth. Not to scale.

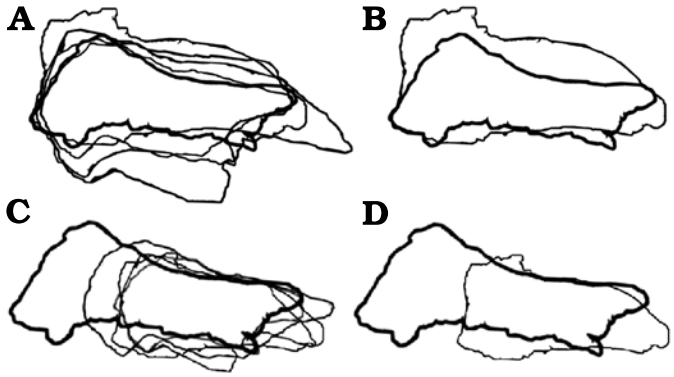

Fig. 7. Björk method of superimposition of the frontals in lateral/medial views. **A**. Scaled to same length between prefrontonasal process and the frontoparietal suture. **B**. Smallest and largest specimen superimposed. **C**. Scaled to same depth near the lacrimal socket region. **D**. Smallest and largest specimen superimposed. Largest specimens preserve entire nasal process, which emphasize relative shortening during growth. Not to scale.

When bone silhouettes are scaled to the same length between prefrontonasal process and parietal suture, increases of relative widths at the postorbital buttress and posterior shelf regions are seen (Fig. 6A–C), supporting the results of bivariate analyses.

Nasal process.—The width of base of the nasal process against the length between the prefrontonasal process and the frontoparietal suture resulted in a slope (Fig. 4A) that is slightly more than 1 (1.224), with the range of 95% confidence intervals that include 1 (0.9119–1.536) with a high correlation coefficient (R^2 = 0.9532, P = 0.0002). These indicate the width of the nasal process isometrically scaled with the length of the

frontal. As noted, the length of the frontal becomes shorter relative to the rest of the bone as the animal's size increases, and isometric growth compared with the length of the bone suggests the nasal process became relatively narrower during growth. This is also supported by a regression of the nasal process width against the width between the orbital slot and the midline of the frontal (Fig. 4B). This regression resulted in a negative slope (0.5188) with significant correlation (R^2 = 0.8203, P = 0.0050), suggesting the width of the nasal process becomes relatively narrower as the rest of the bone widens.

The Björk method of superimposition supports the results. When the silhouettes are superimposed with the same scaled length between the prefrontonasal process and the frontoparietal suture, no clear differences in relative width of the nasal process are observed (Fig. 6A–C). However, when they superimposed with the same scaled width between the orbital slot and the midline of the frontal, a decrease of relative width of the process is found (Fig. 6D–F). These are consistent with isometric scaling with the length of the bone, but negative allometry against the width of the bone.

Prefrontal suture.—The width of the notch between the prefrontonasal and prefrontolacrimal processes (= sutural surface for the prefrontal) resulted in a positive slope (2.383) against the length between the prefrontonasal process and the frontoparietal suture with a high (R^2 = 0.8854) and significant (P = 0.0016) correlation coefficient (Fig. 4C). This suggests the prefrontal suture of the frontal (and probably the prefrontal itself on the skull roof) widened as the length of the frontal increased. When compared with the width between the orbital slot and the midline of the frontal (Fig. 4D), the prefrontal suture shows isometric scaling (slope = 1.043 with the range of 95% confidence intervals 0.4679–1.619) with a high correlation coefficient (R^2 = 0.8130, P = 0.0055), which suggests the widening of the prefrontal suture is largely correlated to the widening of the frontal bone itself.

When the specimen silhouettes are scaled to the same length between the prefrontonasal process and the frontoparietal suture, an increase of relative width of the prefrontal suture (Fig. 6A–C) is found, but when silhouettes are superimposed with the same scaled width between the orbital slot and the midline of the frontal, no clear difference is found (Fig. 6D–F). These results are consistent with those of the bivariate analyses.

Lacrimal socket.—The mediolateral width of the lacrimal socket against the length between the prefrontonasal process and the frontoparietal suture showed strong positive allometry (Fig. 4E), as it resulted in a slope of 2.968 with a high correlation coefficient (R^2 = 0.8459, P = 0.0012). This indicates the width of the lacrimal socket increased significantly as the frontal lengthened. When compared to the width between the orbital slot and the midline (Fig. 4F), the lacrimal socket shows slightly positive allometry (slope = 1.427 with the range of 95% confidence intervals 1.094–1.760) with high (R^2 = 0.9484) and significant (P < 0.0001) correlation coefficient. These results indicate that as the animal grew, the width of the lacrimal socket significantly increased.

Superimposition of specimen silhouettes scaled to the same length between the prefrontonasal process and the frontoparietal suture shows significant increase of relative width of the lacrimal socket (Fig. 6A–C), whereas only slight increase of the relative width is observed when silhouettes are superimposed with the same scaled width between the orbital slot and the midline of the frontal (Fig. 6D–F). These are consistent with the allometric trends found in bivariate analyses.

Postorbital suture.—The anteroposterior length of the postorbital suture increases in size with slightly positive allometry (slope = 1.392 with the range of 95% confidence intervals 1.060–1.724) when compared with the length between the prefrontonasal process and the frontoparietal suture (Fig. 5A) with a high correlation coefficient (R^2 = 0.9461, P < 0.0001), indicating this area increased its relative length during growth. Regressions of depths of both anterior and posterior parts of the postorbital suture (Fig. 5B, C) resulted in slopes much greater than 1 (3.194 and 3.304 respectively) with high correlation coefficients (R^2 = 0.9676, P = 0.0025 for the former; R^2 = 0.8743, P = 0.0197 for the latter). We demonstrate here that the depth of the posterior part of the postorbital suture increased isometrically (Fig. 5D) compared with the depth of the anterior part (Slope = 1.063 with the range of 95% confidence intervals 0.6373–1.489). The correlation coefficient for this was high (R^2 = 0.9546, P = 0.0042). The depths of anterior and posterior parts of the postorbital suture against the depth of the frontal show isometry, as the former (Fig. 5E) resulted in a slope of 0.9688 with the range of 95% confidence intervals 0.1330–1.805 (R^2 = 0.9256, P = 0.0379) and the latter (Fig. 5F) with a slope of 1.272 with the range of 95% confidence intervals 0.6402–1.904 (R^2 = 0.9740, P = 0.0131). These results suggest the deepening of the both parts of the postorbital suture are largely correlated to the deepening of the frontal bone itself.

Dorsotemporal fossa.—The regression of the length of the dorsotemporal fossa against the length of the frontal between the prefrontonasal process and the frontoparietal suture resulted in a slope of 1.941 with a high correlation coefficient (R^2 = 0.9849, P < 0.0001), indicating the coverage of the fossa on the bone increased as the animal grew (Fig. 5G). When compared to the width between the orbital slot and the midline, a negative slope (0.8559) resulted. However, its range of 95% confidence intervals (0.6199–1.092) encompasses 1 (R^2 = 0.9292, P = 0.0001), and the latter factor supports isometric scaling of the dorsotemporal fossa with the width of the bone (Fig. 5H).

Discussion

Ontogenetic stage of specimens.—The dimensions (i.e., the width between the orbital slot and the midline, depth of the bone) of the smallest specimen in the sample, MPC-D 107/10,

are comparable to those of LACM 28471, which is an exceptionally small juvenile specimen of *Tyrannosaurus rex* (Currie 2003b; Carr and Williamson 2004). Recent studies (Erickson et al. 2004; Funston et al. 2021) suggest different species of young tyrannosaurids had similar body sizes at equivalent ages. They also suggest body sizes are consistent with maturity during juvenile–subadult ontogenetic stages of tyrannosaurids (Carr 2020), and these support the juvenile status of MPC-D 107/10. Additionally, results of the Björk superimposition method show MPC-D 107/10 was proportionally shallow in depth and had a relatively wide nasal process. However, it was relatively narrow overall (with a narrow lacrimal socket and was proportionally narrow across both regions of the postorbital suture) compared with other specimens in the sample. According to Carr (1999), Currie (2003b) and Carr and Williamson (2004), these are common features in small juvenile tyrannosaurid frontals.

The Björk method of superimposition results indicate MPC-D 107/05 and MPC-D 107/09 had relatively narrower nasal processes, were wider across the postorbital buttress and posterior shelf, had a wider lacrimal socket, and were relatively deeper in comparison with the slightly smaller MPC-D 107/10. As expected, these indicate these specimens were more mature (Currie 2003b; Hurum and Sabath 2003; Carr and Williamson 2004). However, the dimensions as well as proportions of the postorbital buttress and the posterior shelf, and the frontal depth of these specimens revealed by Björk method of superimposition are intermediate between MPC-D 107/10 and larger, presumably more mature specimens (MPC-D 107/06, 11, 13, 22). Dimensions of MPC-D 107/05 and MPC-D 107/09 are similar to CMNH 7541, a small juvenile *Tyrannosaurus rex* (Carr 1999; Currie 2003b), and based on this and other reasons, these specimens are considered as juveniles as well, albeit more mature than MPC-D 107/10.

The larger specimen MPC-D 107/13 has a proportionally wider lacrimal socket, postorbital buttress and posterior shelf, and a thicker depth of the bone compared to MPC-D 107/05 and MPC-D 107/09 as revealed by the Björk superimposition method. However, its relative depth and widths of postorbital buttress and posterior shelf, as well as its absolute dimensions are still not as great as those of largest specimens (MPC-D 107/06, 22). The dimensions of MPC-D 107/13 are similar to those of LACM 23845 (Currie 2003b), a subadult *Tyrannosaurus rex* (Carr and Williamson 2004; Carr 2020). Considering that adult body sizes of *Tarbosaurus bataar* and *Tyrannosaurus rex* are comparable with each other (Currie 2003a; Holtz 2004), it is reasonable to assume MPC-D 107/13 is from a subadult as well. Dimensions of MPC-D 107/11 are similar to those of MPC-D 107/13, suggesting that it was at an equivalent growth stage when it perished.

MPC-D 107/22 is a large specimen with dimensions significantly greater than those of MPC-D 107/13, but similar to several examples of adult *Tyrannosaurus rex* (Currie 2003b). The Björk method of superimposition shows this specimen has proportionally the widest lacrimal socket, postorbital buttress, posterior shelf and prefrontal suture of all sampled specimens in this work. And for these reasons this specimen of *Tarbosaurus bataar* is considered as an adult (although potentially a young one). MPC-D 107/06 is larger than MPC-D 107/22 in nearly all dimensions, and its proportional depth is the largest of all sampled specimens. Thus, it is considered as an adult as well and is possibly more mature than MPC-D 107/22.

Ontogenetic allometry and variation of *Tarbosaurus bataar* frontals in comparison with other tyrannosaurids.—Overall adult morphologies of the frontal bones in *Tarbosaurus bataar* and *Tyrannosaurus rex* are rectangular outlines that are anteroposteriorly short and mediolaterally wide (Currie et al. 2003; Hurum and Sabath 2003; Carr et al. 2017). Results of bivariate analyses are consistent with ontogenetic mediolateral expansion of the bone (using the orbital slot as a landmark), as mediolateral widths of the postorbital buttress and the posterior shelf both showed positive allometry against the anteroposterior length of the frontal (in which the prefrontonasal process and the frontoparietal suture are used as landmarks). These regions became wider faster as the bone lengthened. These are consistent with the observations of Currie (2003a, b) on various tyrannosaurids, in which the skull roof increased its width during growth. In his comparison of cranial ontogeny in various archosauriforms, Carr (2020) noted the increase of the frontal width of *Tyrannosaurus rex* and predicted *Tarbosaurus bataar* had the same trend. Results of this work show an ontogenetic increase in frontal width is present in *Tarbosaurus bataar* as well.

Indeed, the length of the frontal shows negative allometry when compared to these two variables, and the slopes of them (0.4258 and 0.4372 respectively) are comparable to that (0.48) of Currie (2003b) for tyrannosaurids in general. These indicate the length of the frontal increased in size with negative allometry in *Tarbosaurus bataar*, as it does in other tyrannosaurids (Currie 2003a, b). Currie (2003b) proposed the lengths of the brains of large tyrannosaurid individuals were relatively shorter compared to those of smaller ones (negative allometry). Although the allometric slope of the brain length against the length of the frontal was less than 1, the range of 95% confidence intervals encompasses 1, which indicates isometry between the length of the frontal and the length of the part of the brain associated with the frontal. Currie (2003b) compared brain size with skull length, maxillary tooth row length, and other metrics that are not directly correlated with brain growth the way that the frontal is. Because frontal length is strongly correlated with brain size, it is no surprise that frontal length grows with negative allometry compared with skull length, maxillary tooth row length and other metrics related to total body size.

Allometric slopes of these variables against the length of the bone (between the prefrontonasal process and the frontoparietal suture) are very similar to each other. Bivariate

analyses suggest the postorbital buttress and the posterior shelf scaled isometrically during growth in *Tarbosaurus bataar*. This is a potential difference with albertosaurines and other tyrannosaurines that diverge earlier than the *Tarbosaurus bataar* + *Tyrannosaurus rex* clade. In adult albertosaurine frontals, the widest point is located at the anterior part of the postorbital suture, whereas the widest point is located at the posterior end of the bone in later taxa (Voris 2018). In *Tyrannosaurus rex*, both parts are equal in their width (e.g., Voris 2018), suggesting these variables scaled isometrically like in *Tarbosaurus bataar*. Additional investigations on allometric growth of frontals in multiple tyrannosaurid taxa are needed to clarify whether there were genuine differences between them.

Bivariate analyses regarding the width between the prefrontonasal and prefrontolacrimal processes suggest both processes become widely separated from each other during growth, suggesting widening of the prefrontal and its sutural area on the frontal. Carr (2020) noted the contact surfaces for the prefrontals are narrow in young specimens of *Tyrannosaurus rex*, and the grooves across the dorsum of the prefrontolacrimal and prefrontonasal processes are shallow in juveniles and subadults. Of note, McDonald et al. (2018) named the tyrannosaurine taxon *Dynamoterror dynastes* based on a fragmentary skeleton from the Menefee Formation of New Mexico that preserves parts of both frontals. The only unambiguous autapomorphy of this taxon proposed by McDonald et al. (2018) is that the prefrontonasal and prefrontolacrimal processes are in close proximity and are only separated by a shallow notch. Yun (2020a, b, 2022) proposed that such a feature may represent a subadult character because it is present in the subadults in other tyrannosaurids. Results of this study suggest the presence of relatively narrow prefrontal sutures in immature *Tarbosaurus bataar* frontals. This supports the argument of Yun (2020a, b) that the morphology of the prefrontal joint surface might be inadequate for diagnosis of this taxon, especially when the ontogenetic stage of the holotype is not certain (McDonald et al. 2018). Nevertheless, the age of the approximately 78 Ma type locality indicates the Menefee taxon is probably distinct from all other known tyrannosaurids (McDonald et al. 2018).

The dorsotemporal fossa of a tyrannosaurid skull roof was the origin for adductor jaw musculature (Carr 2020; but see Holliday et al. 2019 for an alternative opinion), and the dorsotemporal ridges in tyrannosaurid frontals mark the anterior margins of the dorsotemporal fossae (Carr et al. 2017; Yun 2020b). The allometric slope of the length of the dorsotemporal fossa against the length of the frontal (between the prefrontonasal process and the frontoparietal suture) showed positive allometry, and the combination of this and the increase in width of the frontal strongly suggests an increase of the muscle attachment area (Carr 2020). This is almost certainly scaling with the amount of the adductor musculature of the jaw, which is massive in large tyrannosaurids (Carr 2020). Carr (2020) found that the dorsotemporal fossa extended anteriorly significantly during growth in *Tyrannosaurus rex*, and the results here show that the same growth trend is found in *Tarbosaurus bataar*.

Depths of the bone in various parts (the medial surface of the bone that is anterior to the sagittal crest, anterior and posterior parts of postorbital suture) also show positive allometry against the anteroposterior length of the frontal (between the prefrontonasal process and the frontoparietal suture), indicating the bone thickened as the animal grew. This is probably to form a solid anchor throughout the skull for the jaw musculature (Currie 2003b). The slope (1.518) for the depth of the frontal compared to the width is similar to that (1.38) of Currie (2003b) for tyrannosaurids in general. Slopes for the depths of the postorbital suture against the medial surface of the bone that is anterior to the sagittal crest suggest isometric relationships between them. This should be treated as provisional, however, as this result may simply be an outcome of small sample size of our dataset (N = 4), which is termed "soft isometry" (Brown and Vavrek 2015).

Comparisons of ontogenetic changes in *Tarbosaurus* frontals with phylogenetic character changes in tyrannosauroids.—The differences found between frontal bones of *Tarbosaurus bataar* of different sizes are also found in early-diverging and later-diverging tyrannosauroids. For example, the Björk method of superimposition as well as bivariate analyses suggest the width of the nasal process grew with negative allometry, and this is congruent with current tyrannosauroid phylogeny in which the narrow nasal process usually occurs in tyrannosaurines that diverge later than Alioramini (Carr and Williamson 2004, 2010; Lehman and Wick 2012). Additionally, the increase of the relative width of the lacrimal socket is supported in both bivariate analyses and the Björk method of superimposition. Both the Björk method of superimposition and bivariate analyses suggest postorbital buttresses and the posterior shelves in the smallest specimens are relatively narrower compared to those in larger specimens. Finally, bivariate analyses and the Björk method of superimposition confirm positive allometric growth of depth during ontogeny.

All of these are congruent with the phylogenetic transition of characters currently recognized in Tyrannosauridae. Whereas early-diverging tyrannosauroids each have a narrow lacrimal socket (Tsuihiji et al. 2012), later-diverging tyrannosauroids like *Bistahieversor sealeyi* and Tyrannosauridae have absolutely and relatively much wider sockets (Lehman and Wick 2012: fig. 11). The overall shapes of the frontals in early-diverging tyrannosauroids are triangular because of the narrow conditions of the postorbital buttresses and the posterior shelves (Tsuihiji et al. 2012). The overall shapes of the frontals are rectangular in later-diverging tyrannosauroids like *Bistahieversor sealeyi* and Tyrannosauridae because of the mediolaterally expanded postorbital buttresses and posterior shelves (Carr and Williamson 2004; Lehman and Wick 2012: fig. 11; Carr et al. 2017; Yun 2020b). Finally, the frontals are shallow dorsoventrally in early-diverging

taxa like *Timurlengia euotica* or *Suskityrannus hazelae* (Averianov and Sues 2012; Tsuihiji et al. 2012; Brusatte et al. 2016; Nesbitt et al. 2019), but are considerably deeper in later-diverging tyrannosauroids (Currie 2003b; Hurum and Sabath 2003; Carr 2020; Yun 2020b). Similar ontogenetic character changes that recapitulate the phylogenetic character transition have been reported in North American tyrannosaurids as well, especially *Tyrannosaurus rex* (Carr 1999, 2020; Carr and Williamson 2004).

Comparative allometry and ontogeny of the non-tyrannosaurid theropod cranial roof.—While the ontogenetic or allometric changes of the cranial roofs of non-avian theropod dinosaurs outside tyrannosaurids are poorly represented in the literature, at least several important inferences can be made for some. Arden et al. (2019) described three spinosaurine frontal bones from Kem Kem beds of Morocco, and found that the largest frontal specimen (FSAC-KK-7715) is relatively shorter but wider compared to the smaller specimens (FSAC-KK-3209, 3210). While differences in the relative depth of the bone are not discussed in the paper, the published figures suggest the larger specimen is relatively deeper as well (Arden et al. 2019: figs. 2, 3). While the spinosaurine affinities of some of these materials were questioned (Ibrahim et al. 2020), a subsequent publication involving some of the same authors accepted the referral of them to a derived spinosaurine (Smyth et al. 2020). These frontals are thought to be from a single taxon (Smyth et al. 2020) or at least two coeval taxa that are very closely related to each other (Arden et al. 2019). While Arden et al. (2019) proposed the smaller specimens described in their work may be from relatively more mature individuals than the larger specimen, based on the bone textures, this is an ambiguous character for assessing ontogeny (e.g., Scannella and Horner 2011) and the differences in texture of those materials may simply be due to preservation status (Smyth et al. 2020). Nevertheless, these suggest an allometric trend that possibly demonstrates ontogeny in spinosaurine frontals, and is similar to that of *Tarbosaurus bataar*. While a landmark-based analysis of Foth et al. (2016) found a relative decrease of the skull height in the frontoparietal region in the ontogeny of megalosaurs, this result may also be due to the dorsally convex postrostral region of the skull of the hatchling *Sciurumimus albersdoerferi* (Rauhut et al. 2012). This convex arching is typical of the youngest archosaurs (Bhullar et al. 2012) and not because of relative decreases in the depths of roofing bones of the skulls themselves.

Loewen (2009) noted a widening of the posterior part of the skull of *Allosaurus fragilis* during ontogeny, and the geometric morphometric comparisons of Foth et al. (2016) found a relative increase of the skull depth in the cranial roof region of this taxon. Large carcharodontosaurid frontals are characterized by their wide and deep nature (Sereno and Brusatte 2008; Cau et al. 2012, 2013), and their maximum lengths are only about 140% of the maximum widths (Sereno and Brusatte 2008). A recent study by Cau (2021) raises the possibility that the holotype individual of *Scipionyx samniticus* is a hatchling carcharodontosaurid, and the frontal of this specimen is thin and narrow but anteroposteriorly elongate (Dal Sasso and Maganuco 2011). Thus, it is inferred that allometric and ontogenetic trends of allosauroid frontals are shortening, widening and deepening of the bone, similar to the trend seen in *Tarbosaurus bataar*.

A juvenile *Megaraptor namunhuaiquii* specimen described by Porfiri et al. (2014) preserves a frontal that is narrow and dorsoventrally shallow. Frontals in a subadult *Murusraptor barrosaensis* are relatively deeper, and the width of the bone is approximately 50% of its length (Coria and Currie 2016). Finally, a large megaraptorid frontal MCF-PVPH-320 is transversely wide, anteroposteriorly short, and remarkably thick (Paulina-Carabajal and Coria 2015; Paulina-Carabajal and Currie 2017). Therefore, it can be assumed that the allometric and perhaps ontogenetic trend of frontal bones in megaraptorids are for relative increases in depth and width with decreases in relative lengths—trends that are also observed in *Tarbosaurus bataar*.

Collectively, these observations suggest ontogenetic allometry of the frontal bones in large, theropod clades such as allosauroids, megaraptorids and spinosaurids compare favorably with patterns seen in *Tarbosaurus bataar*. And as previously mentioned, largely similar allometric trends are present in North American tyrannosaurids as well. Intriguingly, it is known that large carnivorous theropods of different lineages including allosauroids, ceratosaurs, and tyrannosaurids share ontogenetic trends of increasing relative skull heights (e.g., Ratsimbaholison et al. 2016), and these are thought to be convergently acquired (Bhullar et al. 2012). Additional specimens of different growth stages of basal theropod or tetanuran specimens are needed to clarify whether the similarities in ontogenetic and allometric patterns in frontal bones among large theropods are convergent as well, or plesiomorphic. Of note, increase of cranial roof width was recently hypothesized as a plesiomorphic archosauriform growth pattern by Carr (2020), and the relative shortening of the frontal is correlated with the negative allometry associated with growth of organs like the brain and eye, both of which would have had an influence on frontal length (Currie 2003b). Indeed, it has been demonstrated that theropod orbit size is negatively allometric with skull size (e.g., Stevens 2006; Holtz 2008).

Different functional hypotheses have been raised for deep and wide skull roofs of large theropods. Cau et al. (2013) suggested the deepened frontal of the carcharodontosaurid *Sauroniops pachytholus* may indicate agonistic head-butting behavior of this taxon, and a similar idea was proposed for tyrannosaurids (Bakker et al. 1988). However, there is currently no evidence indicating head-butting in tyrannosaurids (Currie 2003a), and pathologies in the cranial roof due to such intraspecific combat are yet to be reported in this clade, unlike pachycephalosaurs (Peterson et al. 2013). Instead, numerous cases of bite marks in large theropod skulls strongly suggest facial biting was a ma-

jor intraspecific aggression behavior (Tanke and Currie 1998; Peterson et al. 2009; Brown et al. 2021). Therefore, head-butting behavior seems to be an unlikely driving force of development of wide, deep cranial roof of large theropods, or at least in tyrannosaurids.

Currie (2003b) suggested the deep nature of tyrannosaurid frontals probably formed an anchor for the jaw musculature, and that the positively allometric growth of frontal width was correlated with a disproportionate increase in the width of the adductor muscles. This is reasonable, as dorsotemporal fossae show extensive growth on tyrannosaurid frontals, especially in large individuals of *Tarbosaurus bataar* and *Tyrannosaurus rex* (Carr et al. 2017; Carr 2020). The allometric increases in jaw musculature are correlated in tyrannosaurids by other indicators of increased bite forces, including greater antorbital skull depths, relatively taller lower jaw heights, and wider basal widths of the maxillary and dentary teeth (Currie 2003a; Brusatte and Carr 2016). While spinosaurids have relatively small dorsotemporal fossae compared to tyrannosaurids, one of the specimens (FSAC-KK-3210) described in Arden et al. (2019) possesses dorsotemporal fossae that are very wide and extensive (Ibrahim et al. 2020). This suggests a considerable amount of jaw adductor musculature covered the cranial roofs of spinosaurids as well. Megaraptoran frontals are characterized by extension of the dorsotemporal fossae onto the dorsal surfaces of the frontals, to similar degrees seen in tyrannosaurids (Porfiri et al. 2014; Paulina-Carabajal and Currie 2017). Finally, while the dorsotemporal fossae of carcharodontosaurid frontals are relatively small in size (Sereno and Brusatte 2008), the presence of an elongate sagittal crest in *Shaochilong maortuensis* suggests the possibility that adductors did considerably cover the dorsal surface of the frontal in this clade (Brusatte et al. 2010). Based on these observations, it is probable that the shared allometric and ontogenetic trends in frontals (widening, deepening) between tyrannosaurids like *Tarbosaurus bataar* and other large theropods are related to thickening the skull roof as an anchor for the disproportionate increase in jaw musculature in adults.

Conclusions

The general ontogenetic changes of the frontal bone of *Tarbosaurus bataar* include an increase in mediolateral width, an increase of the extent of the jaw muscle attachment area (dorsotemporal fossa), and an increase of the depth of the bone. Similar ontogenetic changes have been reported in North American tyrannosaurids, and the results of this study support the changes in the frontal bone of *Tarbosaurus bataar* during growth were similar in all tyrannosaurids. Ontogenetic allometry in various aspects of the frontal also suggest the growth changes in the frontal of *Tarbosaurus bataar* was very similar to that of *Tyrannosaurus rex*, in which both are recapitulating the phylogenetic character transition of the clade Tyrannosauroidea. Lastly, an allometric trend of deepening and widening of tyrannosaurid frontals, exemplified by *Tarbosaurus bataar* in this work, is also seen in various large non-avian theropod clades and these shared trends are hypothesized as related to forming stronger, wider anchors for the jaw adductor musculature.

Acknowledgements

The isolated frontals were collected by members of the Dinosaurs of the Gobi (Nomadic Expeditions) and the Korea–Mongolia International Dinosaur Project funded by grants from the Dinosaur Research Institute (Calgary, Canada), Lee Hunter (Tokyo, Japan), Hwaseong City (South Korea), Albert Miniaci (Ft. Lauderdale, USA), Nathan Myrhvold (Seattle, USA), and NSERC (Discovery Grant RGPIN-2017-04715 to PJC). This manuscript was improved by insightful comments from Thomas Carr (Carthage College, Kenosha, USA), an anonymous reviewer, and the editor Daniel Barta (Oklahoma State University, Tahlequah, USA).

References

Arden, T.M.S., Klein, C.G., Zouhri, S., and Longrich, N.R. 2019. Aquatic adaptation in the skull of carnivorous dinosaurs (Theropida: Spinosauridae) and the evolution of aquatic habits in spinosaurs. *Cretaceous Research* 93: 275–284.

Averianov, A. 2016. Frontal bones of non-avian theropod dinosaurs from the Upper Cretaceous (Santonian–Campanian) Bostobe Formation of the northeastern Aral Sea region, Kazakhstan. *Canadian Journal of Earth Sciences* 53: 168–175.

Averianov, A. and Sues, H.-D. 2012. Skeletal remains of Tyrannosauroidea (Dinosauria: Theropoda) from the Bissekty Formation (Upper Cretaceous: Turonian) of Uzbekistan. *Cretaceous Research* 34: 284–297.

Bakker, R.T., Williams, M., and Currie, P.J. 1988. *Nanotyrannus*, a new genus of pygmy tyrannosaur, from the latest Cretaceous of Montana. *Hunteria* 1: 1–30.

Bever, G.S. Brusatte, S.L., Carr, T.D., Xu, X., Balanoff, A.M., and Norell, M.A. 2013. The braincase anatomy of the Late Cretaceous dinosaur *Alioramus* (Theropoda: Tyrannosauroidea). *Bulletin of the American Museum of Natural History* 376: 1–72.

Bhullar, B.A., Marugan-Lobon, J., Racino, F., Bever, G.S., Rowe, T.B., Norell, M.A., and Abzhanov, A. 2012. Birds have paedomophic dinosaur skulls. *Nature* 487: 223–226.

Brown, C.M. and Vavrek, M.J. 2015. Small sample sizes in the study of ontogenetic allometry; implications for palaeobiology. *PeerJ* 3: e818.

Brown, C.M., Currie, P.J., and Therrien, F. 2021. Intraspecific facial bite marks in tyrannosaurids provide insight into sexual maturity and evolution of bird-like intersexual display. *Paleobiology* [published online, https://doi.org/10.1017/pab.2021.29].

Brusatte, S.L. and Carr, T.D. 2016. The phylogeny and evolutionary history of tyrannosaurid dinosaurs. *Scientific Reports* 6: 20252.

Brusatte, S.L., Averianov, A., Sues, H.-D., Muir, A., and Butler, I.B. 2016. New tyrannosaur from the mid-Cretaceous of Uzbekistan clarifies evolution of giant body sizes and advanced senses in tyrant dinosaurs. *Proceedings of the National Academy of Sciences of the United States of America* 113: 3447–3452.

Brusatte, S.L., Carr, T.D., and Norell, M.A. 2012. The osteology of *Alioramus*, a gracile and long-snouted tyrannosaurid (Dinosauria: Theropoda) from the Late Cretaceous of Mongolia. *Bulletin of the American Museum of Natural History* 366: 1–197.

Brusatte, S.L., Chure, D.J., Benson, R.B.J., and Xu, X. 2010. The osteology of *Shaochilong maortuensis*, a carcharodontosaurid (Dinosauria: Theropoda) from the Late Cretaceous of Asia. *Zootaxa* 2334: 1–46.

Carpenter, K. 2010. Variation in a population of Theropoda (Dinosauria): *Allosaurus* from the Cleveland-Lloyd Quarry (Upper Jurassic), Utah, USA. *Paleontological Research* 14: 250–259.

Carr, T.D. 1999. Craniofacial ontogeny in Tyrannosauridae (Dinosauria, Coelurosauria). *Journal of Vertebrate Paleontology* 19: 497–520.

Carr, T.D. 2010. A taxonomic assessment of the type series of *Albertosaurus sarcophagus* and the identity of Tyrannosauridae (Dinosauria, Coelurosauria) in the *Albertosaurus* bonebed from the Horseshoe Canyon Formation (Campanian–Maastrichtian, Late Cretaceous). *Canadian Journal of Earth Sciences* 47: 1213–1226.

Carr, T.D. 2020. A high resolution growth series of *Tyrannosaurus rex* obtained from multiple lines of evidence. *PeerJ* 8: e9192.

Carr, T.D. and Williamson, T.E. 2004. Diversity of late Maastrichtian Tyrannosauridae (Dinosauria: Theropoda) from western North America. *Zoological Journal of the Linnean Society* 142: 479–523.

Carr, T.D. and Williamson, T.E. 2010. *Bistahieversor sealeyi*, gen. et sp. nov., a new tyrannosauroid from New Mexico and the origin of deep snouts in Tyrannosauroidea. *Journal of Vertebrate Paleontology* 30: 1–16.

Carr, T.D., Varricchio, D.J., Sedlmayr, J.C., Roberts, E.M., and Moore, J.R. 2017. A new tyrannosaur with evidence for anagenesis and a crocodile-like facial sensory system. *Scientific Reports* 7: 44942.

Cau, A. 2021. Comments on the Mesozoic theropod dinosaurs from Italy. *Atti della Società dei Naturalisti e dei Matematici di Modena* 52: 81–95.

Cau, A., Dalla Vecchia, F.M., and Fabbri, M. 2012. Evidence of a new carcharodontosaurid from the Upper Cretaceous of Morocco. *Acta Palaeontologica Polonica* 57: 661–665.

Cau, A., Dalla Vecchia, F.M., and Fabbri, M. 2013. A thick-skulled theropod (Dinosauria, Saurischia) from the Upper Cretaceous of Morocco with implications for carcharodontosaurid cranial evolution. *Cretaceous Research* 40: 251–260.

Coria, R.A. and Currie, P.J. 2016. A new megaraptoran dinosaur (Dinosauria, Theropoda, Megaraptoridae) from the Late Cretaceous of Patagonia. *PLoS ONE* 11: e0157973.

Currie, P.J. 1987. Theropods of the Judith River Formation of Dinosaur Provincial Park, Alberta, Canada. *Tyrrell Museum of Palaeontology, Occasional Papers in Palaeontology* 3: 52–60.

Currie, P.J. 2003a. Allometric growth in tyrannosaurids (Dinosauria: Theropoda) from the Upper Cretaceous of North America and Asia. *Canadian Journal of Earth Sciences* 40: 651–665.

Currie, P.J. 2003b. Cranial anatomy of tyrannosaurid dinosaurs from the Late Cretaceous of Alberta, Canada. *Acta Palaeontologica Polonica* 48: 191–226.

Currie, P.J. 2009. Faunal distribution in the Nemegt Formation (Upper Cretaceous), Mongolia. *In*: Y.-N. Lee (ed.), *Annual Report 2008, Korea-Mongolia International Dinosaur Project*, 143–156. Korean Institute of Geology and Mineralogy, Seoul.

Currie, P.J. 2013. Articulated tyrannosaurid (Dinosauria) skeletons from the Nemegt Formation of Mongolia. *In*: *2013 Hwaseong International Dinosaurs Expedition Symposium, Korea Mongolia International Dinosaur Expedition, December 04–06, 2013*, 26–33. Rolling Hills Hotel, Hwaseong City, Gyeong Province, Korea.

Currie, P.J. 2016. Dinosaurs of the Gobi: Following in the footsteps of the Polish-Mongolian Expeditions. *Palaeontologia Polonica* 67: 83–100.

Currie, P.J. and Dong, Z.M. 2001. New information on *Shanshanosaurus huoyanshanensis*, a juvenile tyrannosaurid (Theropoda, Dinosauria) from the Late Cretaceous of China. *Canadian Journal of Earth Sciences* 38: 1729–1737.

Currie, P.J., Hurum, J.H., and Sabath, K. 2003. Skull structure and evolution in tyrannosaurid dinosaurs. *Acta Palaeontologica Polonica* 48: 227–234.

Dal Sasso, C. and Maganuco, S. 2011. *Scipionyx samniticus* (Theropoda: Compsognathidae) from the Lower Cretaceous of Italy (Osteology, ontogenetic assessment, phylogeny, soft tissue anatomy, taphonomy and palaeobiology). *Memorie della Società Italiana di Scienze Naturali e del Museo Civico di Storia Naturale di Milano* 37: 1–281.

Dalman, S.G., Lucas, S.G., Jasinski, S.E., and Longrich, N.R. 2022. *Sierraceratops turneri*, a new chasmosaurine ceratopsid from the Hall Lake Formation (Upper Cretaceous) of south-central New Mexico. *Cretaceous Research* 130: 105034.

Delcourt, R. and Grillo, O.N. 2018. Tyrannosauroids from the Southern Hemisphere: Implications for biogeography, evolution, and taxonomy. *Palaeogeography, Palaeoclimatology, Palaeoecology* 511: 379–387.

Erickson, G.M., Makovicky, P.J., Currie, P.J., Norell, M.A., Yerby, S.A., and Brochu, C.A. 2004. Gigantism and comparative life-history parameters of tyrannosaurid dinosaurs. *Nature* 430: 772–775.

Evans, D.C., Cullen, T.M., Larson, D.W., and Rego, A. 2017. A new species of troodontid theropod (Dinosauria: Maniraptora) from the Horseshoe Canyon Formation (Maastrichtian) of Alberta, Canada. *Canadian Journal of Earth Sciences* 54: 813–826.

Fiorillo, A.R. and Tykoski, R.S. 2014. A diminutive new tyrannosaur from the top of the world. *PLoS ONE* 9: e91287.

Foth, C., Hedrick, B.P., and Ezcurra, M.D. 2016. Cranial ontogenetic variation in early saurischians and the role of heterochrony in the diversification of predatory dinosaurs. *PeerJ* 4: e1589.

Fowler, D.W., Woodward, H.M., Freedman, E.A., Larson, P.L., and Horner, J.R. 2011. Reanalysis of "*Raptorex kriegsteini*": a juvenile tyrannosaurid dinosaur from Mongolia. *PLoS ONE* 6: e21376.

Funston, G.F., Powers, M.J., Whitebone, S.A., Brusatte, S.L., Scannella, J.B., Horner, J.R., and Currie, P.J. 2021. Baby tyrannosaurid bones and teeth from the Late Cretaceous of western North America. *Canadian Journal of Earth Sciences* 58: 756–777.

Holliday, C.M., Porter, W.R., Vliet, K.A., and Witmer, L.M. 2019. The frontoparietal fossa and dorsotemporal fenestra of archosaurs and their significance for interpretations of vascular and muscular anatomy in dinosaurs. *The Anatomical Record* 303:1060–1074.

Holtz, T.R., Jr. 2004. Tyrannosauroidea. *In*: D.B. Weishampel, P. Dodson, and H. Osmólska (eds.), *The Dinosauria, second edition*, 111–136. University of California Press, Berkeley.

Holtz, T.R., Jr. 2008. A critical reappraisal of the obligate scavenging hypothesis for *Tyrannosaurus rex* and other tyrant dinosaurs. *In*: P. Larson and K. Carpenter (eds.), Tyrannosaurus rex *the Tyrant King*, 371–396. Indiana University Press, Bloomington.

Hone, D.W., Wood, D., and Knell, R.J. 2016. Positive allometry for exaggerated structures in the ceratopsian dinosaur *Protoceratops andrewsi* supports socio-sexual signaling. *Palaeontologia Electronica* 19: 1–13.

Hurum, J.H. and Sabath, K. 2003. Giant theropod dinosaurs from Asia and North America: Skulls of *Tarbosaurus bataar* and *Tyrannosaurus rex* compared. *Acta Palaeontologica Polonica* 48: 161–190.

Ibrahim, N., Sereno, P.C., Varricchio, D.J., Martill, D.M., Dutheil, D.B., Unwin, D.M., Baidder, L., Larsson, H.C.E., Zouhri, S., and Kaoukaya, A. 2020. Geology and paleontology of the Upper Cretaceous Kem Kem Group of eastern Morocco. *ZooKeys* 928: 1–216.

Jerzykiewicz, T., Currie, P.J., Fanti, F., and Lefeld, J. 2021. Lithobiotopes of the Nemegt Gobi Basin. *Canadian Journal of Earth Sciences* 58: 829–851.

Knapp, A., Knell, R.J., and Hone, D.W.E. 2021. Three-dimensional geometric morphometric analysis of the skull of *Protoceratops andrewsi* supports a socio-sexual signalling role for the ceratopsian frill. *Proceedings of the Royal Society B: Biological Sciences* 288: 20202938.

Lehman, T.M. and Wick, S.T. 2012. Tyrannosauroid dinosaurs from the Aguja Formation (Upper Cretaceous) of Big Bend National Park, Texas. Earth and Environmental Science *Transactions of the Royal Society of Edinburgh* 103: 471–485.

Loewen, M.A. 2009. *Variation in the Late Jurassic Theropod Dinosaur* Allosaurus*: Ontogenetic, Functional, and Taxonomic Implications*. 342 pp. Unpublished Ph.D. Dissertation, University of Utah, Salt Lake City.

Loewen, M.A., Irmis, R.B., Sertich, J.W., Currie, P.J., and Sampson, S.D. 2013. Tyrant dinosaur evolution tracks the rise and fall of Late Cretaceous oceans. *PLoS ONE* 8: e79420.

Longrich, N.R. 2008. A new, large ornithomimid from the Dinosaur Park Formation of Alberta, Canada: Implications for the study of dissociated dinosaur remains. *Palaeontology* 51: 983–997.

Lü, J., Yi, L., Brusatte, S.L., Yang, L., Li, H., and Chen, L. 2014. A new clade of Asian Late Cretaceous long-snouted tyrannosaurids. *Nature Communications* 5: 3788.

Maleev, E.A. 1955a. Gigantic carnivorous dinosaurs from Mongolia [in Russian]. *Doklady AN SSSR* 104: 634–637.

Maleev, E.A. 1955b. New carnivorous dinosaurs from the Upper Cretaceous of Mongolia [in Russian]. *Doklady AN SSSR* 104: 779–782.

McDonald, A.T., Wolfe, D.G., and Dooley, A.C. 2018. A new tyrannosaurid (Dinosauria: Theropoda) from the Upper Cretaceous Menefee Formation of New Mexico. *PeerJ* 6: e5749.

Nesbitt, S.J., Denton, R.K., Loewen, M.A., Brusatte, S.L., Smith, N.D., Turner, A.H., Kirkland, J.I., McDonald, A.T., and Wolfe, D.G. 2019. A mid-Cretaceous tyrannosauroid and the origin of North American end-Cretaceous dinosaur assemblages. *Nature Ecology & Evolution* 3: 892–899.

Paul, G.S., Persons, W.S., and Van Raalte, J. 2022. The tyrant lizard king, queen and emperor: Multiple lines of morphological and stratigraphic evidence support subtle evolution and probable speciation within the North American genus *Tyrannosaurus*. *Evolutionary Biology* [published online, https://doi.org/10.1007/s11692-022-09561-5].

Paulina-Carabajal, A. and Coria, R. 2015. An unusual theropod frontal from North Patagonia. *Alcheringa* 39: 514–518.

Paulina-Carabajal, A. and Currie, P.J. 2017. The braincase of the theropod dinosaur *Murusraptor*: Osteology, neuroanatomy and comments on the paleobiological implications of certain endocranial features. *Ameghiniana* 54: 617–640.

Paulina-Carabajal, A., Currie, P.J., Dudgeon, T.W., Larsson, H.C., and Miyashita, T. 2021. Two braincases of *Daspletosaurus* (Theropoda: Tyrannosauridae): anatomy and comparison. *Canadian Journal of Earth Sciences* 58: 885–910.

Peterson, J.E., Dischler, C., and Longrich, N.R. 2013. Distributions of cranial pathologies provide evidence for head-butting in dome-headed dinosaurs (Pachycephalosauridae). *PLoS ONE* 8: e68620.

Peterson, J.E., Henderson, M.D., Scherer, R.P., and Vittore, C.P. 2009. Face biting on a juvenile tyrannosaurid and behavioral implications. *Palaios* 24: 780–784.

Porfiri, J.D., Novas, F.E., Calvo, J.O., Agnolin, F.L., Ezcurra, M.D., and Cerda, I.A. 2014. Juvenile specimen of *Megaraptor* (Dinosauria, Theropoda) sheds light about tyrannosauroid radiation. *Cretaceous Research* 51: 35–55.

Rauhut, O.W.M., Foth, C., Tischlinger, H., and Norell, M.A. 2012. Exceptionally preserved juvenile megalosauroid theropod dinosaur with filamentous integument from the Late Jurassic of Germany. *Proceedings of the National Academy of Sciences* 109: 11746–11751.

Ratsimbaholison, N.O., Felice, R.N., and O'Connor, P.M. 2016. Ontogenetic changes in the craniomandibular skeleton of the abelisaurid dinosaur *Majungasaurus crenatissimus* from the Late Cretaceous of Madagascar. *Acta Palaeontologica Polonica* 61: 281–292.

Rozhdestvensky, A.K. [Rožděstvenskij, A.K] 1965. Growth changes and some problems of systematics of Asian dinosaurs [in Russian]. *Paleontologičeskij žurnal* 1965 (3): 95–109.

Russell, D. 1970. Tyrannosaurs from the Late Cretaceous of western Canada. *National Museum Natural Sciences Publications in Palaeontology* 1: 1–34.

Saveliev, S. and Alifanov, V. 2007. A new study of the brain of the predatory dinosaur *Tarbosaurus bataar* (Theropoda, Tyrannosauridae). *Paleontological Journal* 41: 281–289.

Scannella J.B. and Horner J.R. 2011. "*Nedoceratops*": An example of a transitional morphology. *PLoS ONE* 6: e28705.

Schneider, C.A., Rasband, W.S., and Eliceiri, K.W. 2012. NIH Image to ImageJ: 25 years of image analysis. *Nature Methods* 9: 671–675.

Sereno, P.C. and Brusatte, S.L. 2008. Basal abelisaurid and carcharodontosaurid theropods from the Lower Cretaceous Elrhaz Formation of Niger. *Acta Palaeontologica Polonica* 53: 15–46.

Sereno, P.C., Tan, L., Brusatte, S.L., Kriegstein, H.J., Zhao, X., and Cloward, K. 2009. Tyrannosaurid skeletal design first evolved at small body size. *Science* 326: 418–422.

Smyth, R.S., Ibrahim, N., and Martill, D.M. 2020. *Sigilmassasaurus* is *Spinosaurus*: a reappraisal of African spinosaurines. *Cretaceous Research* 114: 104520.

Stevens, K.A. 2006. Binocular vision in theropod dinosaurs. *Journal of Vertebrate Paleontology* 26: 321–330.

Tanke, D.H. and Currie, P.J. 1998. Head-biting behavior in theropod dinosaurs: paleopathological evidence. *Gaia* 15: 167–184.

Tsuihiji, T., Watabe, M., Tsogtbaatar, K., Barsbold, R., and Suzuki, S. 2012. A tyrannosauroid frontal from the Upper Cretaceous (Cenomanian–Santonian) of the Gobi Desert, Mongolia. *Vertebrata PalAsiatica* 50: 102–110.

Tsuihiji, T., Watabe, M., Tsogtbaatar, K., Tsubamoto, T., Barsbold, R., Suzuki, S., Lee, A.H., Ridgely, R.C., Kawahara, Y., and Witmer, L.M. 2011. Cranial osteology of a juvenile specimen of *Tarbosaurus bataar* (Theropoda, Tyrannosauridae) from the Nemegt Formation (Upper Cretaceous) of Bugin Tsav, Mongolia. *Journal of Vertebrate Paleontology* 31: 497–517.

Voris, J.T. 2018. *Cranial Anatomy and Ontogeny of* Gorgosaurus libratus *(Tyrannosauridae: Albertosaurinae).* 115 pp. M.Sc. Thesis, University of Calgary, Calgary.

Voris, J.T., Zelenitsky, D.K., Therrien, F., and Currie, P.J. 2019. Reassessment of a juvenile *Daspletosaurus* from the Late Cretaceous of Alberta, Canada with implications for the identification of immature tyrannosaurids. *Scientific Reports* 9: 17801.

Voris, J.T., Therrien, F., Zelenitsky, D.K., and Brown, C.M. 2020. A new tyrannosaurine (Theropoda: Tyrannosauridae) from the Campanian Foremost Formation of Alberta, Canada, provides insight into the evolution and biogeography of tyrannosaurids. *Cretaceous Research* 110: 104388.

Warton, D.I., Wright, I.J., Falster, D.S., and Westoby, M. 2006. Bivariate line-fitting methods for allometry. *Biological Reviews* 81: 259–291.

Yun, C.-G. 2020a. A reassessment of the taxonomic validity of *Dynamoterror dynastes* (Theropoda: Tyrannosauridae). *Zoodiversity* 54: 259–264.

Yun, C.-G. 2020b. A subadult frontal of *Daspletosaurus torosus* (Theropoda: Tyrannosauridae) from the Late Cretaceous of Alberta, Canada with implications for tyrannosaurid ontogeny and taxonomy. *PalArch's Journal of Vertebrate Palaeontology* 17: 1–13.

Yun, C.-G. 2022. Frontal bone anatomy of *Teratophoneus curriei* (Theropoda: Tyrannosauridae) from the Upper Cretaceous Kaiparowits Formation of Utah. *Acta Palaeontologica Romaniae* 18: 51–64.